A Modification of the Garrett–Munk Internal Wave Spectrum

MURRAY D. LEVINE

College of Oceanic and Atmospheric Sciences, Oregon State University, Corvallis, Oregon

(Manuscript received 24 October 2001, in final form 25 April 2002)

ABSTRACT

The Garrett–Munk (GM) spectrum continues to be a useful description of the oceanic internal wave field. However, there are several inconsistencies and ambiguities that make it difficult to use in comparing internal wave fields at different latitudes, stratifications, and water depths. A modified spectral formulation is presented that treats three problems with the Garrett–Munk formulation: the normalization of the energy spectrum as a function of frequency bandwidth, the energy distribution at frequencies below the semidiurnal tide, and the treatment of vertical boundaries and turning points. Addressing these problems leads to a substitution of the GM parameters E (nondimensional energy), b (vertical length scale), and N_0 (buoyancy frequency scale) with two new dimensional scales: E_{ref}, the energy per unit mass, and $D(\omega)$, the Wentzel–Kramers–Brillouin (WKB)-scaled thickness of the vertical waveguide. The advantages of the modified spectrum are illustrated by comparing with observations from the equator and the continental shelf.

1. Introduction

The Garrett–Munk spectrum (Garrett and Munk 1972, 1975) continues to be a useful description of the oceanic internal wave field, particularly of the deep, open ocean. [GM is used to refer to the general Garrett–Munk spectrum; GM79 is the term used for the specific form presented in Munk (1981).] The GM spectrum is often used as a representative statistical description of the internal wave field in studies of nonlinear interaction (e.g., Müller et al. 1986; Hibiya et al. 1998), acoustic propagation (e.g., Colosi et al. 1999; Flatté 1979), and mixing parameterization (e.g., Henyey et al. 1986; Polzin 1995). It has permeated the literature and is used in ways that sometimes exceed its applicability. The particular distribution of waves in frequency–wavenumber space given by GM is significant, but most remarkable is that there exists any frequency–wavenumber distribution that appears to be ''universal'' in space and time. Of course, this universality is not exact, and it is the deviations that can provide clues to explain the generation, propagation, and dissipation of the waves (e.g., Wunsch 1975; Müller and Briscoe 1999). The value of a spectral formulation, which is consistent with the kinematics of internal waves, is that it permits comparisons among any of the measurable statistical quantities. It is then possible to relate, for example, a velocity frequency spectrum observed at buoyancy frequency $N = N_1$ with a horizontal wavenumber spectrum of vertical displacement at $N = N_2$.

In order to make meaningful comparisons between observations in different environments, the application of the spectral formulation must be unambiguous and consistent. The purpose of this paper is to present a modified spectral formulation of the internal wave field that addresses three problematic aspects of the GM description regarding: the normalization of the energy spectrum as a function of the frequency bandwidth, the energy distribution at frequencies below the semidiurnal tide, and the treatment of vertical boundaries and turning points. These problems have lead to ambiguous interpretations of the scaling parameters in the GM formulation, especially when applied to observations from different latitudes, buoyancy frequency profiles, and water depths.

In GM79 the spectrum is normalized such that the total energy is not a function of f when integrated over all frequencies from f to N. This results in a frequency spectrum that scales as f—a dependence that is not observed. This shortcoming is acknowledged in GM79 and Munk (1980), and it is suggested that this scaling by f be replaced by the constant value of f at 30°N (f_{30}). While this indeed removes the f dependence in the spectral level, it is no longer consistent to maintain that the integral of the frequency spectrum from local f to N is constant with latitude. We suggest an alternate consistent normalization, referenced to the spectral level of the high frequencies only, which has the desired property of eliminating the f dependence on the spectral level while no longer constraining the integrated energy from f to N to be constant.

We also suggest a modification of the spectral distribution of the energy for frequencies less than $\omega_{S_2} = 1/12$ cph, the principal semidiurnal solar tidal frequency.

Corresponding author address: Dr. Murray D. Levine, 104 Ocean Admin. Bldg., Oregon State University, Corvallis, OR 97331.
E-mail: levine@coas.oregonstate.edu

This change is motivated by observations at low latitude that indicate a whiter frequency spectrum below the semidiurnal tidal band (e.g., Eriksen 1980). There may also be dynamical reasons for this change in spectral slope, suggesting the tide as an energy source to the internal wave continuum (e.g., Munk and Wunsch 1998; Levine et al. 1983).

Regarding the treatment of the vertical dependence of the internal wave field in a spectral formulation, there are two issues of importance. One is the method of solution of the vertical structure equation, and the other is the assumption of statistical independence between waves. In a flat-bottom ocean the exact solution of the vertical structure can be represented as a set of discrete vertical modes, essentially vertical standing waves resulting from the imposition of upper and lower boundary conditions. It is often more convenient to use a nonexact, Wentzel–Kramers–Brillouin (WKB) solution of the equation, which ignores the boundaries and treats the wave field as a sum of vertically propagating waves. The modal representation of a stationary and horizontally homogeneous random wave field requires that waves of different modes, horizontal wavenumbers, and frequencies be statistically independent. In propagating WKB solutions it is usually assumed that upward and downward propagating waves are independent (e.g., Müller et al. 1978). Differences in the specification of statistical independence between propagating and standing solutions lead to different behavior of the statistical quantities (e.g., Müller and Siedler 1976). It is even possible to combine aspects of both propagating and standing solutions (e.g., Blumenthal and Briscoe 1995). The GM spectrum essentially ignores the boundaries and uses a form similar to the WKB approximation. In the modified spectral form presented here, we choose to include the effects of the boundaries and turning points while retaining the analytical advantages of the WKB approximation. This representation of vertical structure is called *WKB modes* and is especially useful in application to the shallow ocean where the boundaries may be important at even relatively high frequencies.

These problems in the GM formulation can also lead to uncertain interpretation of the three GM scaling parameters: E, the nondimensional energy parameter; b, the vertical length scale; and N_0, the buoyancy frequency scale. It is not possible to compare internal wave observations with the GM spectrum when it is not clear how to estimate the values of these scaling parameters from the data. One approach is to consider the GM spectrum as a benchmark of the universal, deep-ocean internal wave field by using the GM canonical values of E (6.3×10^{-5}), b (1300 m), and N_0 (3 cph). This is a useful procedure for comparing the energy and coherence pattern of an observed wave field with a typical deep-ocean wave field.

A second approach is to use the observed spectra and coherences collectively to set the values of these scaling parameters. The difficulty is that there are a variety of different procedures that could be used to estimate the GM parameters, thereby leading to a nonunique determination of values from a given set of observations. For example, should the scales b and N_0 be estimated from the $N(z)$ profile only, or should other data be used as well? Part of the problem is that only two of the parameters are independent in the spectral formulation (Desaubies 1976). In the modified formulation we replace the three GM scales with two new dimensional parameters: E_{ref}, the energy per unit mass, and $D(\omega)$, the scaled thickness of the vertical waveguide. These two parameters are defined so that they can be determined in a straightforward manner from observations of any bottom depth with any reasonable $N(z)$ profile. The objective of this approach is to clarify the procedure for comparing diverse internal wave fields.

We begin section 2 with a review of the general statistical framework of a random internal wave field. Suggested modifications of the GM79 description are then presented. In section 3 observable spectral quantities, such as spectra and coherences, are derived for this modified formulation and compared with GM79. The new formulation is applied to some observations in section 4. The advantages of this new approach are discussed and summarized in section 5.

2. Theoretical framework

A sum of random, linear internal waves on an f plane can be expressed as a random process (following Schott and Willebrand 1973 and Willebrand et al. 1977) as

$$u^L(x, y, z, t) = \int_f^{N_{\max}} \int_{-\infty}^{+\infty} \int_{-\infty}^{+\infty} A(\omega, k, l) p^L(\omega, \theta) \times q^L(z, \omega, \alpha) e^{i(kx+ly-\omega t)}\, dk\, dl\, d\omega + \text{c.c.}, \quad (1)$$

where the u^L vector represents the eastward velocity, northward velocity, and buoyancy-scaled vertical displacement ($N\zeta$) for $L = 1$, 2, and 3, respectively. In addition, ω is the frequency, and k and l are the horizontal wavenumbers in the x and y direction, respectively. The magnitude of the horizontal wavenumber is α, the angle of the wavenumber vector counterclockwise from east is θ, the spectral measure of the random process is A, and

$$p^L(\omega, \theta) = \left[\frac{(i\omega\cos\theta - f\sin\theta)}{\omega}, \frac{(i\omega\sin\theta + f\cos\theta)}{\omega}, i\right]$$

$$q^L(z, \omega, \alpha) = \left(\frac{1}{\alpha}\frac{\partial\psi}{\partial z}, \frac{1}{\alpha}\frac{\partial\psi}{\partial z}, \psi\frac{N(z)}{\omega}\right).$$

Only positive ω needs to be considered. The depth de-

pendence given by $\psi(z)$ satisfies the vertical structure equation

$$\frac{d^2\psi}{dz^2} + \alpha^2\frac{N^2(z) - \omega^2}{\omega^2 - f^2}\psi = 0. \quad (2)$$

Horizontal velocity could alternatively be expressed as a counterclockwise rotary component (+) for $L = 1$ and a clockwise component (−) for $L = 2$ by changing p^L to

$$p^L(\omega, \theta) = \left[\frac{(\omega - f)(i\cos\theta + \sin\theta)}{\sqrt{2}\omega}, \frac{(\omega + f)(i\cos\theta - \sin\theta)}{\sqrt{2}\omega}, i\right]. \quad (3)$$

We assume that the random wave field is statistically stationary and horizontally homogeneous, which implies that the x, y, and t dependence of

$$C^{LM}(\Delta x, \Delta y, z_1, z_2, \tau) = \langle u^L(x, y, z_1, t)u^M(x + \Delta x, y + \Delta y, z_2, t + \tau)\rangle \quad (4)$$

is a function only of Δx, Δy, and τ, where angle brackets represent the expected value. This requires that amplitudes between waves of different k, l, and ω be statistically independent:

$$\langle A(\omega, k, l)A(\omega', k', l')\rangle = 0$$
$$\langle A(\omega, k, l)A^*(\omega', k', l')\rangle = E_c(\omega, k, l)\delta(\omega - \omega')\delta(k - k')\delta(l - l'), \quad (5)$$

where $E_c(\omega, k, l)$ is the spectral energy distribution function in Cartesian wavenumber.

Imposing rigid level boundaries on (2) at the surface ($z = 0$) and the bottom ($z = -H$) results in vertically standing waves described by a discrete set of eigenvectors

$$\psi_j \equiv \psi(\omega, \alpha_j)$$

with associated eigenvalues $\alpha = \alpha_j(\omega)$ that satisfy the orthogonality relationship

$$\int_{-H}^{0} \psi_j\psi_k\frac{N^2(z) - f^2}{\omega^2 - f^2}\,dz = Q(\omega)\delta_{jk}, \quad (6)$$

where $Q(\omega)$ is the normalization function, which will be defined in the next section. Often waves are described as vertically propagating or a combination of standing and propagating (Blumenthal and Briscoe 1995) even though it does not satisfy the boundary conditions. The choice affects the spectral quantities that depend upon the assumptions of whether there is statistical independence between standing waves of different modes or between propagating waves of different wavenumbers. Here we have chosen to use vertically standing waves to capture explicitly the effects of the boundaries. Then the frequency cross-spectrum between u^L at z_1 and u^M at z_2 can be expressed as

$$S^{LM}(\Delta x, \Delta y, z_1, z_2, \omega) = \int C^{LM}(\Delta x, \Delta y, z_1, z_2, \tau)e^{-i\omega\tau}\,d\tau. \quad (7)$$

The cross-spectrum can then be written in polar coordinates as a function of horizontal separation of distance Δr and angle ϕ:

$$S^{LM}(\Delta r, \phi, z_1, z_2, \omega) = \frac{1}{2\pi}\int_0^{2\pi}\sum_{j=1} T^{LM}(\omega, \theta)R_j^{LM}(z_1, z_2, \omega)E(\omega, \theta, j)e^{-i[\alpha_j(\omega)\Delta r\cos(\theta - \phi)]}\,d\theta, \quad (8)$$

where E is the spectral energy distribution as a function of frequency, wavenumber direction, and mode number:

$$T^{LM}(\omega, \theta) = p^{L^*}(\omega, \theta)p^M(\omega, \theta),$$
$$R_j^{LM}(z_1, z_2, \omega) = q^{L^*}(z_1, \omega, \alpha_j)q^M(z_2, \omega, \alpha_j).$$

Note that the integral over k and l has been replaced by an integral over θ and a sum over modes j.

a. Normalization of E and ψ

The normalization function $Q(\omega)$ in (6) is usually chosen by appealing to the energy equation. Using (8), the frequency spectrum at depth z of the total energy per unit mass is given by

$$\Upsilon(\omega, z) = \text{KE} + \text{PE} = \frac{1}{2\pi}\int_0^{2\pi}\sum_j G(z, \omega, j)E(\omega, \theta, j)\,d\theta, \quad (9)$$

where KE is the kinetic energy $\frac{1}{2}(u^2 + v^2 + w^2)$ and PE is the potential energy $\frac{1}{2}N^2\zeta^2$ and

$$G(z, \omega, j) = \left[\frac{\omega^2 + f^2}{2\omega^2}\left(\frac{\psi_j'}{\alpha_j}\right)^2 + \frac{N^2 + \omega^2}{2\omega^2}\psi_j^2\right].$$

The vertical integral of Υ in (9) can then be written as

$$\int_{-H}^{0}\Upsilon(\omega, z)\,dz = \frac{1}{2\pi}\int_0^{2\pi}\sum_j\left[\int_{-H}^{0} G(z, \omega, j)\,dz\right]E(\omega, \theta, j)\,d\theta = \frac{1}{2\pi}\int_0^{2\pi}\sum_j Q(\omega)E(\omega, \theta, j)\,d\theta \quad (10)$$

using (2) and (6). The choice of $Q(\omega)$ for normalization determines the dimensions and definitions of both $E(\omega,$

θ, j) and ψ. Usually $Q(\omega) = 1$ (dimensionless), which then sets the quantity $\rho_0 E(\omega, \theta, j)$ to be the total energy per unit area per unit frequency at mode j and direction θ (e.g., Müller et al. 1978). However, we choose to normalize ψ such that $E(\omega, \theta, j)$ has units of energy per unit mass (rather than area) per unit frequency at mode j and direction θ, since this quantity appears to be more universal than energy per unit area. Hence, $Q(\omega)$ has units of length; we choose $Q(\omega)$ to be a vertical scale representative of the waveguide thickness, which will be defined in the next section.

b. WKB modes

To study the general depth dependence of ψ, it is instructive to use the WKB approximate solution of (2) (e.g., Neyfeh 1973) given by

$$\psi(z) \simeq N(z)^{-1/2} e^{\pm i\gamma(z)}, \tag{11}$$

where

$$\gamma(z) = \int_{z_L}^{z} \frac{\alpha N(z)}{(\omega^2 - f^2)^{1/2}}\, dz \tag{12}$$

and the hydrostatic approximation has been made; that is, $N^2 - \omega^2 \approx N^2$. Both upward and downward propagating phases are permitted, indicated by the $\pm$ in the exponent, respectively. This solution is oscillatory between lower and upper turning depths z_L and z_U, defined by $N(z_L) = N(z_U) = \omega$. Because of the hydrostatic and WKB approximations, the solution is more accurate away from the turning points, that is, for $\omega \ll N(z)$. For simplicity we have assumed a smooth N profile with at most two turning depths. If there are no turning depths, that is, $\omega < N(z)$ everywhere in the water column, then $-H$ and 0 are used for z_L and z_U, respectively. It is useful to express (12) in terms of a stretched vertical coordinate ξ:

$$\gamma(z) = \frac{\alpha N_{\text{ref}}}{(\omega^2 - f^2)^{1/2}} \xi(z), \tag{13}$$

where

$$\xi(z) = \frac{1}{N_{\text{ref}}} \int_{z_L}^{z} N(z)\, dz. \tag{14}$$

The vertical scaling is then defined relative to a constant reference buoyancy frequency N_{ref}. Any value of N_{ref} could be used without changing the essence of the parameterization; we use 3 cph (5.23×10^{-3} s^{-1}) for easy comparison with GM. The maximum value of ξ is defined to be $D(\omega)$:

$$D(\omega) = \xi(z_U),$$

which is the waveguide thickness in stretched units at frequency ω.

To confine the wave solution to the vertical waveguide created by the boundaries and turning points, we apply a rigid boundary to the WKB solution (11) at the top and bottom of the waveguide. This, of course, is not the correct boundary condition at the turning points and hence yields only approximate solutions which we call *WKB modes*.

We choose to set $Q(\omega) = D(\omega)$ as a reasonable vertical scale of the waveguide. Then the WKB modes using (11) and (13) can be written as

$$\psi_j(z) = \left[\frac{2(\omega^2 - f^2)}{N(z) N_{\text{ref}}}\right]^{1/2} \sin\left[j\pi \frac{\xi(z)}{D(\omega)}\right] \quad \text{and} \tag{15}$$

$$\frac{\psi_j'(z)}{\alpha_j} = \left[\frac{2N(z)}{N_{\text{ref}}}\right]^{1/2} \cos\left[j\pi \frac{\xi(z)}{D(\omega)}\right], \tag{16}$$

where

$$\alpha_j = \frac{j\pi}{D(\omega)} \frac{(\omega^2 - f^2)^{1/2}}{N_{\text{ref}}}. \tag{17}$$

These modes are normalized using (6) after making the simplification $N^2 - f^2 \approx N^2$, which is consistent with the hydrostatic assumption. The wave functions are assumed to have a zero value outside the waveguide. The z dependence of the wave functions are sines and cosines relative to the stretched coordinate ξ and modulated by an additional $N(z)$ dependence. These WKB modal solutions deviate the greatest from the exact solution near $\omega = N(z)$ where the boundary condition is obviously incorrect. Also, as with all WKB solutions, the accuracy depends on the scale of the variation of $N(z)$ and the mode number j.

A more precise analytic approximation would involve using Airy functions near the turning points to patch between the oscillatory and exponential solutions (Desaubies 1973). However, the solution becomes too complicated to make much progress analytically. To improve the approximation, it is easier in practice to use the exact numerical solution of (2) without the need to make the hydrostatic approximation. To permit a consistent comparison with spectral quantities that are estimated using the WKB approximation, the exact modes ψ should be normalized such that $Q(\omega)$ also equals $D(\omega)$—the same as for WKB modes.

For comparison with WKB modes, the GM79 vertical dependence can be expressed essentially as a WKB solution of vertically propagating waves with the deep ocean stratification taken to be

$$N(z) = N_0 e^{z/b} \tag{18}$$

(Table 1). In deriving the spectral quantities, GM assume that $H \gg b$, $\omega \ll N_0$, and z is always far from the top and bottom boundary. Under these assumptions the frequency and H dependence of the waveguide is eliminated, yielding $\xi_{\text{GM79}}(z) = be^{z/b}$ and $D_{\text{GM79}} = b$. The argument of the exponential in the GM79 version of the WKB approximation (12) then becomes

TABLE 1. Comparison of important quantities and parameters between GM79 and the modified spectrum.

Quantity	GM79		Modified spectrum	
$N(z)$	$N(z) = N_0 e^{z/b}$	(18)	No specific form; limit of two turning points $z_L(\omega)$, and $z_U(\omega)$	
Water depth, H	Not explicit; $H \gg b$		Explicitly incorporated in $D(\omega)$	
Vertical waveguide thickness, WKB scaled	b, relative to N_0		$D(\omega) = \frac{1}{N_{\text{ref}}} \int_{z_L}^{z_U} N(z)\, dz$ relative to N_{ref}	(14)
Spectral energy distribution function, $E(\omega, \theta, j)$	$Eb^2 N_0^2 B(\omega) H(j)$	(22)	$E_{\text{ref}} \hat{B}(\omega) H(j)$	(26)
Frequency dependence	$B(\omega)$	(24)	$\hat{B}(\omega)$	(27)
Modal dependence	$H(j)$	(23)	$H(j)$	(23)
Vertical structure	$\psi_{\text{GM79}} = \left[\frac{\omega^2 - f^2}{N(z)N_0}\right]^{1/2} e^{\pm i\gamma_{\text{GM79}}}$		$\psi_j(z) = \left[\frac{2(\omega^2 - f^2)}{N(z)N_{\text{ref}}}\right]^{1/2} \sin\left[j\pi \frac{\xi(z)}{D(\omega)}\right]$	(15)
	$\frac{\psi'_{\text{GM79}}}{\alpha} = \pm i \left[\frac{N(z)}{N_0}\right]^{1/2} e^{\pm i\gamma_{\text{GM79}}}$	(21)	$\frac{\psi'_j(z)}{\alpha_j} = \left[\frac{2N(z)}{N_{\text{ref}}}\right]^{1/2} \cos\left[j\pi \frac{\xi(z)}{D(\omega)}\right]$	(16)
	where $\gamma(z)_{\text{GM79}} \simeq \alpha_{\text{GM79}} \frac{N(z)}{(\omega^2 - f^2)^{1/2}} b$	(19)		
Energy per unit mass (vertically averaged over waveguide thickness)	$Eb^2 N_0^2$ (total from f to N)	(31)	E_{ref} (total from ω_{S_2} to N_{ref})	(32)
Energy per unit area	$\rho_0 Eb^3 N_0^2$	(33)	$\rho_0 E_{\text{ref}} \int_f^{N_{\max}} D(\omega)\hat{B}(\omega)\, d\omega$	(34)

$$\gamma(z)_{\text{GM79}} = \alpha_{\text{GM79}} \frac{N(z) - N(z_L)}{(\omega^2 - f^2)^{1/2}} b \simeq \alpha_{\text{GM79}} \frac{N(z)}{(\omega^2 - f^2)^{1/2}} b, \quad (19)$$

where

$$\alpha_{\text{GM79}} = \frac{j\pi}{b} \frac{(\omega^2 - f^2)^{1/2}}{N_0}. \quad (20)$$

The GM79 wave functions consistent with the same normalization used in (6) are then

$$\psi_{\text{GM79}} = \left[\frac{\omega^2 - f^2}{N(z)N_0}\right]^{1/2} e^{\pm i\gamma_{\text{GM79}}} \quad \text{and}$$

$$\frac{\psi'_{\text{GM79}}}{\alpha} = \pm i \left[\frac{N(z)}{N_0}\right]^{1/2} e^{\pm i\gamma_{\text{GM79}}}. \quad (21)$$

An example comparing the vertical structure of WKB modes (15) and (16) with the exact modes and GM79 wave functions (21) are shown in Fig. 1 for exponential stratification (18). At low frequency, WKB and exact modes are nearly the same. As expected at higher frequency, the WKB modes deviate the greatest from the exact solution near the turning point.

c. Spectral energy distribution function, E(ω, θ, j)

Given a statistical framework for the internal wave field, the challenge has been to choose the functional form of $E(\omega, \theta, j)$ that is most consistent with observations. The fact that a single function can explain many of the properties of the world's internal wave observations is remarkable and is the basis for the success of the GM spectrum. There are a number of versions of E in the literature (e.g., Müller et al. 1978). We use as the standard for comparison the form presented as GM79 in units of energy per unit mass:

$$E_{\text{GM79}}(\omega, \theta, j) = Eb^2 N_0^2 B(\omega) H(j), \quad (22)$$

where

$$H(j) = J \frac{1}{(j^2 + j_*^2)}, \qquad \frac{1}{J} \equiv \sum_1^\infty \frac{1}{j^2 + j_*^2} \quad (23)$$

$$B(\omega) = \frac{2}{\pi} \frac{f}{\omega(\omega^2 - f^2)^{1/2}}. \quad (24)$$

This distribution is horizontally isotropic, that is, independent of θ. The frequency and modal dependence are written as separable functions, even though this does not necessarily agree with some observations (e.g., Pinkel 1984). The j_* parameter is directly related to the wavenumber bandwidth; a larger j_* indicates that the lower modes contribute relatively less to the total energy, thereby increasing the bandwidth. The contribution from higher modes ($j \gg j_*$) rolls off as j^{-2}. It is important to note that at high frequency ($\omega \gg f$) $B(\omega) \sim f$, a consequence of normalizing $B(\omega)$ such that

$$\int_f^{N(z)} B(\omega)\, d\omega = \frac{2}{\pi} \arccos\frac{f}{N} \approx 1. \quad (25)$$

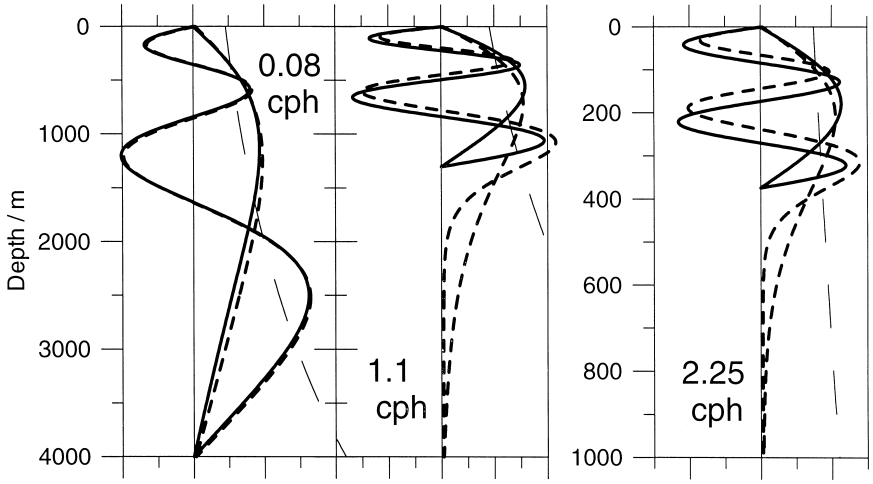

FIG. 1. Vertical structure functions $\psi(z)$ for modes 1 and 4 for the exponential stratification (18) given by Garrett and Munk (1972). The exact solution of (2) (short dashed line) is compared with the WKB mode solution (15) (solid line) and the GM79 envelope (21) (long dashed line), for (left) 0.08, (center) 1.1, and (right) 2.25 cph.

This leads to a frequency spectral level that scales as f—implying that the spectrum decreases rapidly as the equator is approached. As mentioned previously, Munk (1981) notes that this is contrary to observational evidence and suggests a quick fix by scaling the spectrum by f_{30} rather than f. This is equivalent to replacing the f with f_{30} in the numerator of $B(\omega)$ in (24). Then, this leaves open the question: what is the lower limit of integration of $B(\omega)$ in (25)? If it is local f, then the integral of $B(\omega)$ is no longer normalized to 1 and is latitudinally dependent (Fig. 2). If the lower limit is replaced with f_{30}, then it is normalized to 1, but then does the spectrum exist at frequencies below f_{30}? This inconsistency is fundamental: both the spectral level and the total variance (integral of the spectrum) cannot be constant with latitude if the lower limit f varies with latitude. Whatever normalization is used, it must be applied consistently.

We introduce a modified spectral energy distribution function, called E_*, which is intended to clarify the application to general stratification and ocean depth as well as fix inconsistencies in the latitudinal dependence:

$$E_*(\omega, \theta, j) = E_{\text{ref}}\hat{B}(\omega)H(j), \tag{26}$$

where E_{ref} is a constant with dimensions energy per unit mass and

$$\hat{B}(\omega) = \frac{\pi}{2}\frac{B(\omega)}{C}\begin{cases} 1 & \omega_{S_2} < \omega \\ \left(1 + \dfrac{f}{\omega_{S_2}}\right)\dfrac{(\omega/\omega_{S_2})^3}{(\omega/\omega_{S_2})^{2.5} + (f/\omega_{S_2})} & f < \omega < \omega_{S_2} \end{cases}. \tag{27}$$

The bulky analytical form of $\hat{B}$ is empirically derived and chosen for analytical convenience. The normalization constant C is determined by imposing

$$\int_{\omega_{S_2}}^{N_{\text{ref}}} \hat{B}(\omega)\, d\omega = 1, \tag{28}$$

and is given by

$$C = \arccos\frac{f}{N_{\text{ref}}} - \arccos\frac{f}{\omega_{S_2}}.$$

This normalization essentially removes the f dependence of the spectral level at frequencies above ω_{S_2} and thereby makes the integral of $\hat{B}$ over the entire frequency range from f to N_{ref} greater than 1 (Fig. 2). Note, however, that the latitudinal variation of this integral is much less than GM79 with a constant f_{30}. The frequency dependence of $B(\omega)$ has also been modified so that the spectral slope is whiter at frequencies below the semidiurnal tidal frequency ω_{S_2}. The break in spectral slope at ω_{S_2} is based on observations (section 4), although the frequency of the break cannot be determined precisely from the data.

We have assumed a sharp low-frequency cutoff at $\omega = f$ as was done in GM79, essentially ignoring the latitudinal dependence on the wave structure. Since f

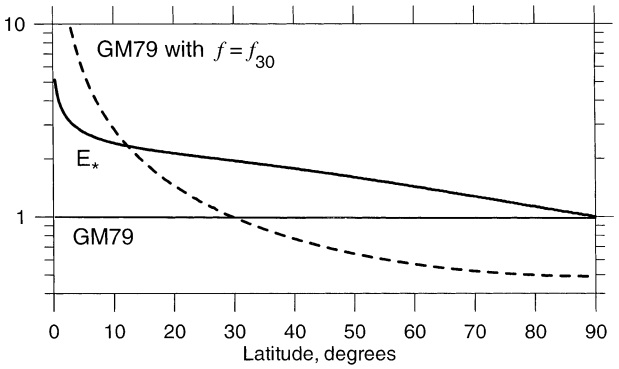

FIG. 2. The integral from f to N of $\hat{B}(\omega)$ in (27) (bold solid line), $B(\omega)$ in (24) (thin solid line), and $B(\omega)$ with $f = f_{30}$ in the numerator (dashed line) as a function of latitude.

is a function of latitude, the more accurate treatment of the latitudinal dependence of the wavefunctions leads to a turning point in latitude. This results in a peak near f and penetration of the exponential tail of waves to latitudes above the turning latitude. Munk (1980) explores the modification of the GM spectrum when this is taken into account. This approach seems to explain the detailed shape of the peak near f (the so-called inertial cusp). Rather than complicate the spectral form, GM parameterize this peak in a less precise manner in $B(\omega)$. The modified spectrum also includes this cusp in an ad hoc manner to avoid analytical complications. For detailed analysis of the near-inertial band see Munk (1980) and Fu (1981).

d. Average energy

Using the specific forms of E_{GM79} in (22) and E_* in (26) and the hydrostatic approximation, the frequency spectrum of total energy per unit mass Υ [(9)] becomes

$$\Upsilon_{\mathrm{GM79}}(\omega, z) = Eb^2 N_0 N(z) B(\omega) \tag{29}$$

$$\Upsilon_*(\omega, z) = E_{\mathrm{ref}} \frac{N(z)}{N_{\mathrm{ref}}} \hat{B}(\omega) \times \sum_j H(j) \left[\frac{\omega^2 + f^2}{\omega^2} \cos^2\left(\frac{j\pi}{D(\omega)} \xi(z) \right) + \frac{\omega^2 - f^2}{\omega^2} \sin^2\left(\frac{j\pi}{D(\omega)} \xi(z) \right) \right]. \tag{30}$$

Note that even though GM79 uses discrete modes in E_{GM79} [(22)], the vertical structure in (21) is usually assumed to be smoothed vertically, thereby eliminating explicit dependence of the vertical structure on mode number. Essentially, the oscillations with depth due to $\exp(i\gamma_{\mathrm{GM79}})$ in (21) are ignored in spectral estimates, but retained in determining vertical coherences. In both forms $\Upsilon \sim N(z)$, but with WKB modes the depth dependence has an additional factor reflecting the boundary conditions. To compare the two forms (Table 1), it is useful to calculate the vertically averaged energy frequency spectrum by dividing the total energy by the vertical waveguide thickness:

TABLE 2. Commonly measured statistical quantities as a function of frequency (ω), vertical mode (j), horizontal wavenumber (k) vs time lag (τ), depths (z), and horizontal separation (Δr). The names of the quantities are derived from D: dropped, M: moored, T: towed, V: vertical, H: horizontal, L: lagged (time), S: spectrum, and/or C: coherence.

	Auto-spectra	Coherences τ, time lag	z_1, z_2	Δr
ω	MS(ω)		MVC(ω, z_1, z_2)	MHC (ω, Δr)
j	DS(j)	DLC(j, τ)		DHC (j, Δr)
k	TS(k)	TLC(k, τ)	TVC(k, z_1, z_2)	

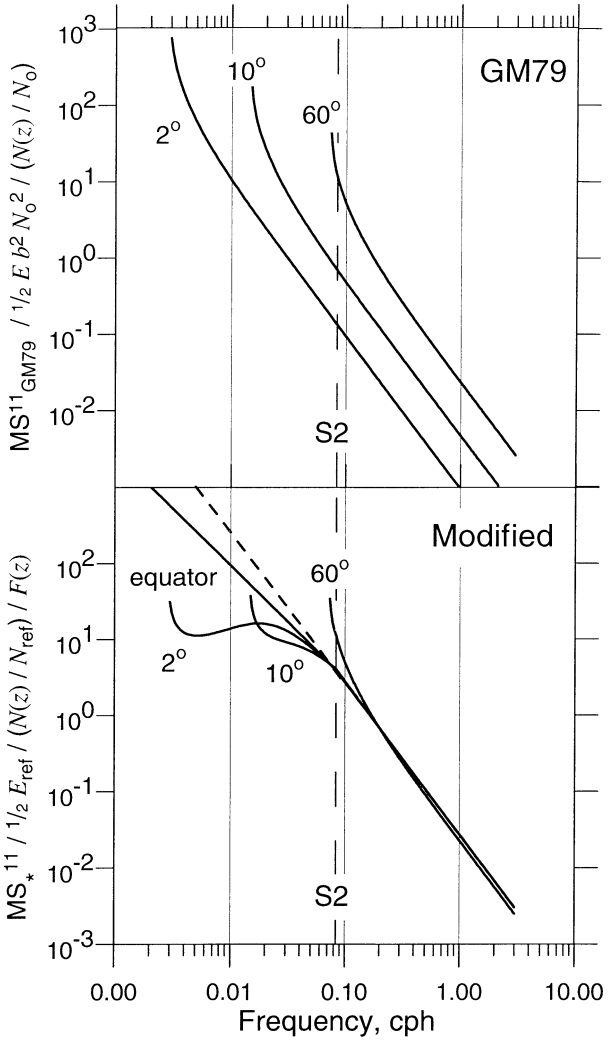

FIG. 3. Moored spectrum (MS) of horizontal velocity at different latitudes for (top) GM79 [(A4)] and (bottom) the modified spectrum [(A5)]. For reference the ω^{-2} slope is shown (dashed line). The function $F(z)$ is shown in Fig. 4.

$$\frac{1}{b}\int_{-H}^{0} \Upsilon_{\mathrm{GM79}}(\omega, z)\, dz = Eb^2N_0^2B(\omega), \qquad f < \omega < N(z) \quad (31)$$

$$\frac{1}{D(\omega)}\int_{z_L(\omega)}^{z_U(\omega)} \Upsilon_*(\omega, z)\, dz = E_{\mathrm{ref}}\hat{B}(\omega), \qquad f < \omega < N_{\max}. \quad (32)$$

From (31), $Eb^2N_0^2$ can be seen to represent the vertically averaged energy per unit mass over the frequency band from f to N by using normalization (25), and from (32) E_{ref} can also be identified as the vertically averaged energy per unit mass over the frequency band from ω_{S_2} to N_{ref} by using (28). It is also clear from the definition of $D(\omega)$ that E_{ref} is the spectral level referenced to the buoyancy frequency N_{ref}. If N_{ref} is changed, so is E_{ref}; E_{ref} is essentially the dimensional spectral level WKB-scaled to $N = N_{\mathrm{ref}}$. Although the choice of N_{ref} is arbitrary, once chosen, it must remain fixed, to enable meaningful comparisons of values of E_{ref} from different environments.

For the GM79 and modified spectra, the energy per unit area can be obtained from (31) and (32), respectively, by integrating over ω and multiplying by density ρ_0:

$$E_{A_{\mathrm{GM79}}} \simeq \rho_0 Eb^3N_0^2 \quad (33)$$

$$E_{A_*} = \rho_0 E_{\mathrm{ref}} \int_f^{N_{\max}} D(\omega)\hat{B}(\omega)\, d\omega. \quad (34)$$

For the modified spectrum the total energy per unit area is a more complicated expression than for GM79 as it depends upon $D(\omega)$, which is a function of $N(z)$. Note also that unlike GM79, E_{A*} is a function of the frequency bandwidth and hence is a strong function of f. At lower latitudes E_{A*} increases, since the energy is assumed constant in the band ω_{S_2} to N_{ref}.

3. Spectral quantities

The ultimate usefulness of the formulation presented in section 2 is determined by comparing with observations. Given sufficient observations, the function $E(\omega, \theta, j)$ could be checked directly. However, typically a more limited set of data is available from which to calculate statistical quantities, revealing only a portion of the functional dependence of $E(\omega, \theta, j)$. The set of the more commonly measured statistical quantities is given in Table 2, along with the terminology originally used by GM.

From (8), the most commonly used spectral quantities—moored spectrum (MS), dropped spectrum (DS), moored horizontal coherence (MHC), and moored vertical coherence (MVC)—can be written

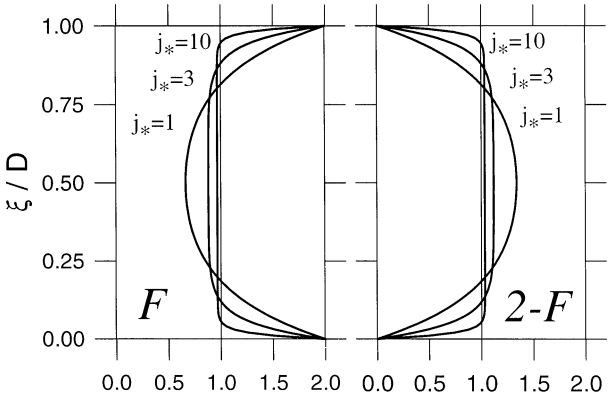

FIG. 4. (left) The factor F [(A2)] that scales velocity MS$_*$ and (right) the factor $(2 - F)$ that scales the vertical displacement MS$_*$ as a function of ξ/D for several values of j_*.

$$\mathrm{MS}^{LM}(\omega, z) = S^{LM}(\Delta r = 0, \phi, z, z, \omega) \quad (35)$$

$$\mathrm{DS}^{LM}(j) = \int_f^{N_{\max}} \left[\frac{1}{2\pi}\int_0^{2\pi} T^{LM}(\omega, \theta)E(\omega, \theta, j)\, d\theta\right] \times \left[\frac{1}{D(\omega)}\int_{z_L}^{z_U} R_j^{LM}(z, z, \omega)\, dz\right] d\omega \quad (36)$$

$$\mathrm{MHC}^{LM}(\omega, \Delta r, \phi, z) = \frac{S^{LM}(\Delta r, \phi, z, z, \omega)}{[MS^{LL}(\omega, z)MS^{MM}(\omega, z)]^{1/2}} \quad (37)$$

$$\mathrm{MVC}^{LM}(\omega, z_1, z_2) = \frac{S^{LM}(\Delta r = 0, \phi, z_1, z_2, \omega)}{[MS^{LL}(\omega, z_1)MS^{MM}(\omega, z_2)]^{1/2}}. \quad (38)$$

These statistical quantities are evaluated for E_* and E_{GM79} in the appendix; some have convenient analytical forms, others contain integrals and sums. The differences between GM79 and the modified spectrum are discussed below.

a. Moored spectrum (MS)

Frequency autospectra of horizontal velocity are shown in Fig. 3 for GM79 [(A4)] and the modified spectrum [(A5)] for several latitudes. The plotted spectra are normalized by factors that depend on z. In GM79 the horizontal velocity spectra scale simply like $N(z)$. In the WKB modal representation, the depth dependence also depends upon the factor F [(A2)], which is a function of $N(z)$, ω, and j_* (Fig. 4). The deviation from the simpler GM79 form of the WKB scaling is greater at lower j_* and near the boundaries or turning points ($\xi = 0$ and 1). Since the spectral level in GM79 scales with f, the variance (integral over all frequencies) is constant for all latitudes. In the E_* formulation, the spectral level at frequencies above ω_{S_2} is normalized to

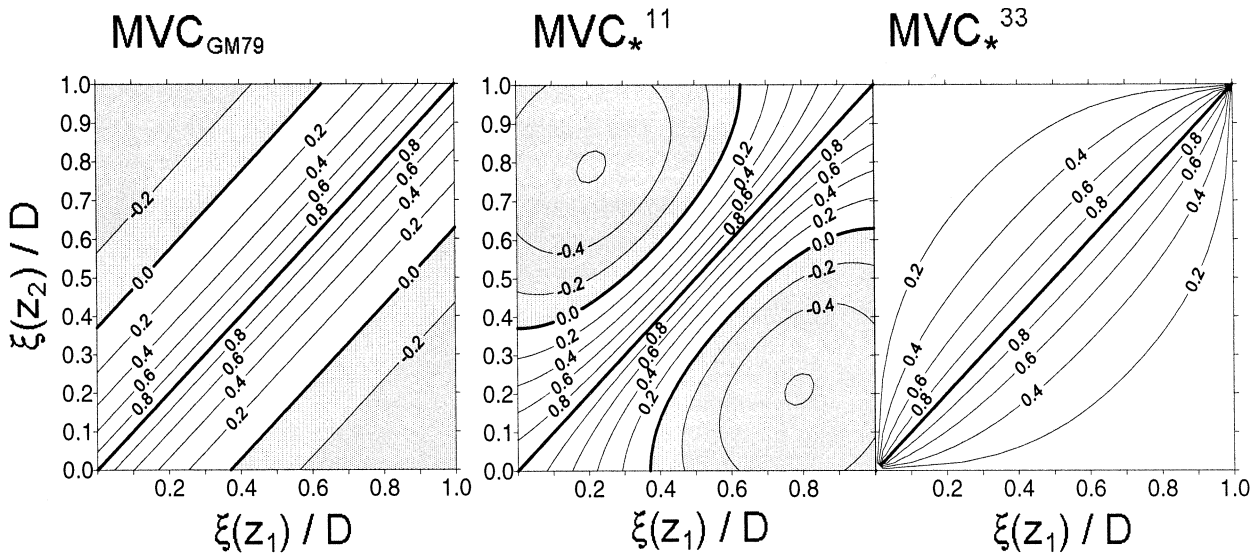

FIG. 5. Moored vertical coherence (MVC) for $j_* = 1$ between depth $\xi(z_1)$ and $\xi(z_2)$ for (left) GM79 [(A12)], (center) the modified spectrum for horizontal velocity [(A13)], and (right) the modified spectrum for vertical displacement [(A14)]. Note that the MVC for velocity and displacement is the same for GM79 but different for the modified spectrum. The corresponding phase spectrum is 0 for positive coherence and π for negative coherence.

be nearly constant and, hence, the total variance increases at lower latitudes.

The shape of the MS_* differs markedly from MS_{GM79} at frequencies below ω_{S_2}. This modification is based on comparisons with observed MS at low latitudes, shown in section 4.

b. Dropped spectrum (DS)

The DS, as a function of mode number, goes like $H(j)$ for both GM79 and E_* [(A8)–(A11)] with the variance given by the sum over all modes. The levels of the spectra, however, are different because of the different functional form and normalization of the frequency dependence; the difference is greatest at lower latitudes. Often the DS is presented as a function of a local vertical wavenumber rather than mode number. From the WKB form (11) a local vertical wavenumber $m(z)$ can be defined as

$$m_{\text{WKB}}(z) = \frac{\partial}{\partial z}\gamma(z). \tag{39}$$

Then the vertical wavenumber for GM79 and the modified spectra become

$$m_{\text{GM79}}(z) = \alpha_{\text{GM79}}\frac{N(z)}{(\omega^2 - f^2)^{1/2}} = \frac{j\pi}{b}\frac{N(z)}{N_0} \quad \text{and} \tag{40}$$

$$m_*(z) = \frac{j\pi}{D(\omega)}\frac{N(z)}{N_{\text{ref}}}. \tag{41}$$

In the modified spectrum, the vertical scale is given by D, a measure of the actual waveguide, rather than the constant b. Remember that the validity of interpreting $m(z)$ as a vertical wavenumber improves as $N(z)$ varies more slowly with depth.

c. Moored vertical coherence (MVC)

The MVC for horizontal velocity and vertical displacement are shown in Fig. 5 for both GM79 and E_* for $j_* = 1$. Since the values of the corresponding phase spectrum can only be 0 or π, they are displayed as positive and negative coherences, respectively. The depth is plotted in terms of the scaled stretched variable $\xi/D(\omega)$. In GM79 the vertical coherence depends only upon differences in ξ and is the same for both horizontal velocity and vertical displacement. For the E_* formulation near the boundaries of the waveguide, the coherences are slightly higher for velocity and slightly lower for displacement. At higher j_* the overall coherence would decrease as the energy is more evenly distributed among the lower modes. At lower j_*, the coherence would be more dominated by mode 1, leading to significant negative velocity coherence between two depths which straddle the zero-crossing of mode 1.

4. Application to observations

In this section the modified E_* spectra are compared with observations to illustrate the latitudinal dependence and to show the application to shallow water. Comparisons with the GM79 spectrum are also made.

a. Low-latitude observations

The E_* and GM79 spectra are compared with observed moored spectra near 9°N and on the equator in

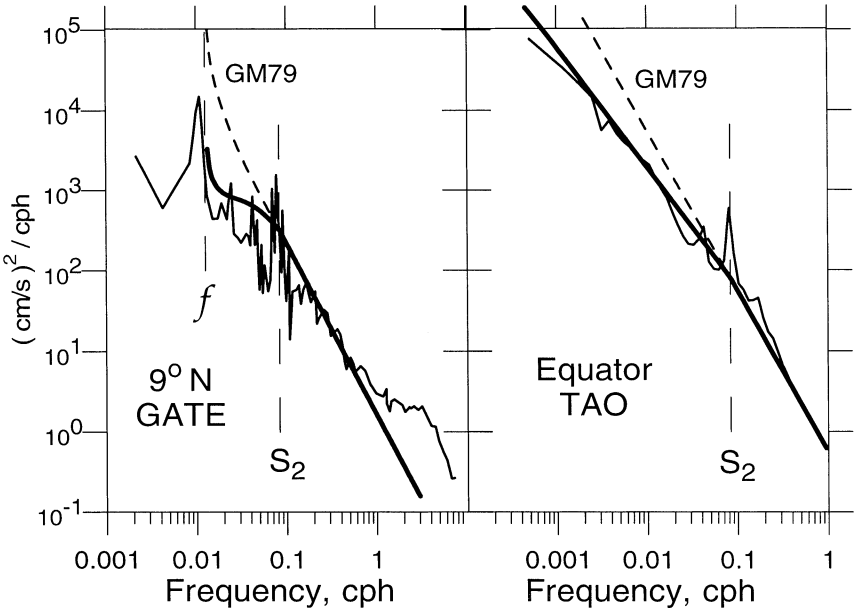

FIG. 6. Moored spectra (MS) of horizontal velocity (thin solid line) observed from (left) 9°N (GATE) and (right) the equator (TAO) are compared with GM79 with $f = f_{30}$ (dashed line) and modified spectrum (bold solid line).

Fig. 6. The spectrum at 9°N (8°49.9′N, 22°52.6′W) is from a mooring deployed for three weeks in 1974 during the GARP Atlantic Tropical Experiment (GATE) at a depth of 56 m in the Atlantic Ocean with a water depth of 4800 m (Käse and Siedler 1979). The equatorial data (140°W) are from a 6-month time series recorded at depth 200 m in 1988 on a mooring of the Tropical Atmosphere–Ocean project (TAO) maintained by the National Oceanic and Atmospheric Administration in the Pacific Ocean (e.g., McPhaden et al. 1998). Both the GM79 and modified spectrum have been scaled subjectively to fit the observed spectra. At frequencies above the semidiurnal band, an ω^{-2} curve fits both sets of observations reasonably well. The spectrum at GATE shows enhanced energy above about 0.7 cph as is typical in many upper ocean measurements (e.g., Levine et al. 1983). Below the semidiurnal frequency, the spectral slope is significantly whiter than GM79. This was noted by Eriksen (1980) in describing data from the equator; others have also commented on this apparent change in spectral slope below the semidiurnal tidal band (e.g., Fu 1981; Pinkel et al. 1987; Levine 1991). The spectral shape specified by $\hat{B}$ reasonably reproduces the behavior below the semidiurnal tide. These few examples do not confirm the universality of this specific spectral form; a more comprehensive study would be required.

The level of these observed frequency spectra can be used to estimate E_{ref} by considering the range $\omega \gg \omega_{S_2}$ in (A5), where

$$\text{MS}_{*}^{11} \simeq E_{\text{ref}} \frac{1}{2} \frac{N(z)}{N_{\text{ref}}} \frac{\omega_{S_2}}{\omega^2} F\left(\frac{\xi}{D}\right). \tag{42}$$

Using the observed $N(z)$, $N_{\text{ref}} = 3$ cph, and assuming a value of $F = 1$, the values of E_{ref} are 1.1 and 2.0 mJ kg^{-1} for data from 9°N and the equator, respectively, as plotted in Fig. 6. For comparison the GM79 moored velocity spectrum in the deep ocean at $\omega \gg \omega_{S_2}$ in (A4) is proportional to f:

$$MS_{\text{GM79}}^{11} \simeq \frac{1}{\pi} Eb^2 N_0 N(z) \frac{f}{\omega^2}. \tag{43}$$

It is obvious, as noted previously, that the observed spectral level does not scale with f. If instead we replace f with a constant f_{30} in the GM79 formulation (recognizing that this is inconsistent) and equate spectra from (39) and (40), then

$$E_{\text{ref}} = \frac{2}{\pi} Eb^2 N_0 N_{\text{ref}} \frac{f_{30}}{\omega_{S_2}} = 0.92 \text{ mJ kg}^{-1}. \tag{44}$$

Hence, the observed values of E_{ref} inferred from the frequency spectra are very close to that predicted from GM79 with $f = f_{30}$—within a factor of about 2. This is not surprising as GM79 with f_{30} is expected to predict the high-frequency spectral level in the deep ocean.

b. Continental shelf observations

To demonstrate the usefulness for application to environments quite different from the deep ocean, the modified spectral formulation is compared with some observations on the continental shelf. Velocity time series were recorded on a mooring in water depth 70 m in the Mid-Atlantic Bight made during the Primer/

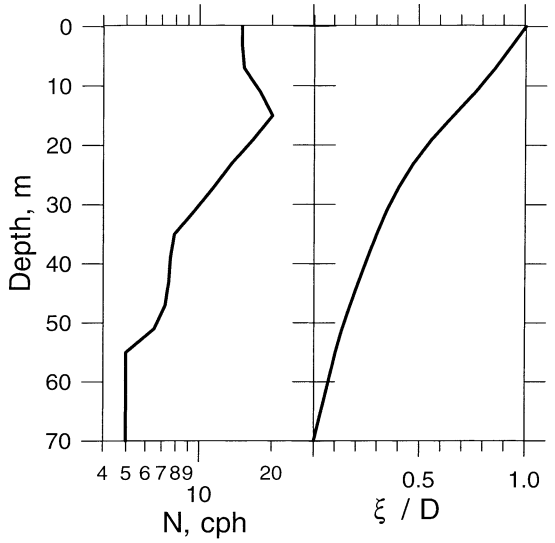

FIG. 7. (left) Buoyancy frequency profile from the Mid-Atlantic Bight during the Primer/CMO experiment 1997, and (right) the corresponding calculation of ξ/D from (14), where $D = 241$ m and $\omega < N_{\min}$ (no turning points).

Coastal Mixing and Optics experiment (CMO) in 1997 (Boyd et al. 1997). An average $N(z)$ profile representative of the stratification from day 210 to 240 is shown in Fig. 7; the corresponding ξ profile (14) is also shown.

The rotary velocity spectra from a depth of 55 m are compared with the modified spectral form in Fig. 8. The spectrum of random internal waves is meant to apply to the internal wave continuum, which in this case, appears to range from the semidiurnal tide to about 0.7 cph. The shape in this continuum band specified by $\hat{B}$ fits the observed spectrum well, which is not very different from GM79 since f and ω_{S_2} are relatively close. The peaks at the tide and inertial frequencies and the spectral shoulder at high frequency are not part of the continuum spectrum. The high-frequency signal is partly due to nonlinear internal wave packets generated at the shelf break traveling shoreward (Boyd and Levine 2002, unpublished manuscript), and partly due to the background random waves (e.g., Levine 1999). It may be possible to incorporate some of these features into the spectral form; however, the study of the high-frequency band is left for another time.

Using the observed spectral levels of the continuum, an estimate of the product $E_{\text{ref}}F$ at each depth can be made using (42) (Fig. 9). The profile of $E_{\text{ref}}F$ as a function of ξ/D is similar in behavior to the function F (Fig. 4) with maxima at the top and bottom. The value of E_{ref} can be estimated by using $F(\xi/\text{D})$ for various choices of j_* (Fig. 9). The value of $j_* = 1$ provides a nearly constant value with depth of $E_{\text{ref}} = 0.85$ mJ kg^{-1}. This value is remarkably near the E_{ref} found for the deep ocean.

Next, the observed vertical coherence structure of the continuum is compared with the E_* and GM79 spectral

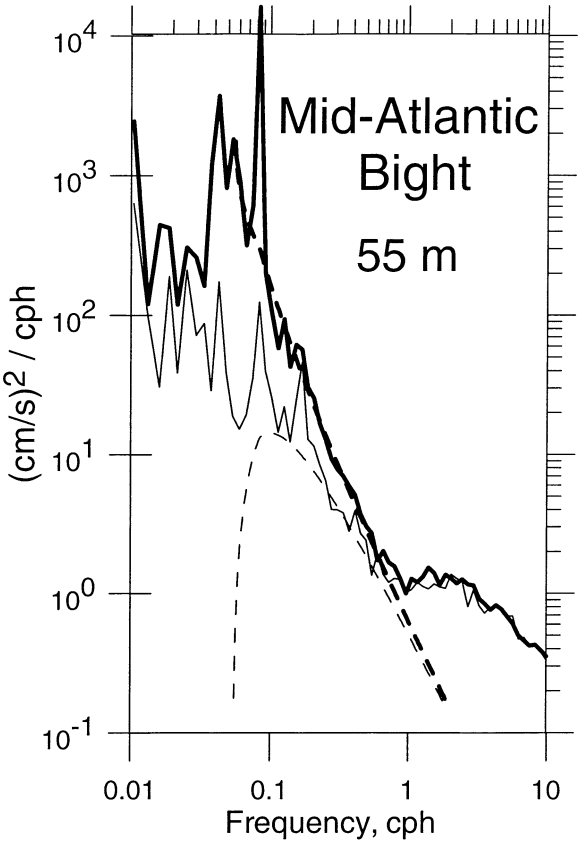

FIG. 8. The clockwise (bold line) and counterclockwise (thin line) rotary spectral components at 55 m depth from the Mid-Atlantic Bight during the Primer/CMO experiment. The modified spectrum MS_*, which is nearly the same shape as GM79 at this latitude, is plotted with the level adjusted for best fit.

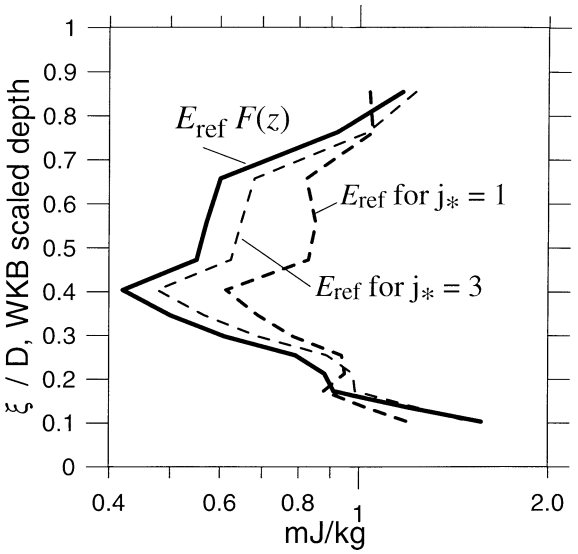

FIG. 9. Vertical profile of $E_{\text{ref}}F(z)$ (solid line) calculated from fitting the observed MS measured during Primer/CMO at different depths to the modified spectral form. Estimates of E_{ref} are obtained by dividing by the function $F(z)$ for $j_* = 3$ (thin dashed line) and $j_* = 1$ (bold dashed line).

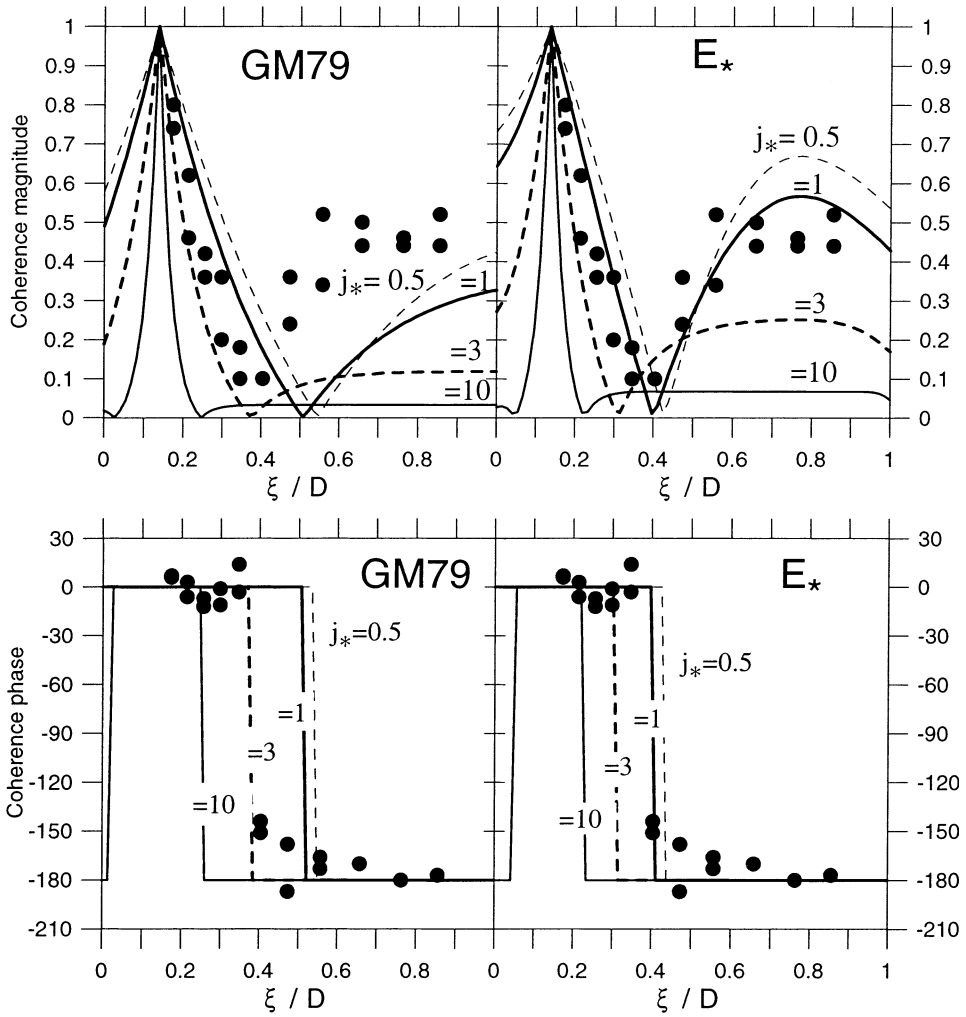

FIG. 10. (top) Coherence and (bottom) phase at 0.5 cph between velocity at 51 m and other depths during the Primer/CMO experiment (dots) are compared with (left) GM79 and (right) the modified spectral form for $j_* = 0.5$, 1, 3, and 10. Depth is scaled as ξ/D (Fig. 7).

forms in Fig. 10. The coherence shown is at a frequency of 0.5 cph between velocities at 51 m ($\xi/D = 0.10$) and all other depths. The observations clearly agree better with the modified spectrum than GM79. The primary difference between the coherences of the two forms is at large vertical separation—the E_* formulation predicts a larger coherence magnitude due to the effects of boundaries on WKB modes. The best agreement of the E_* formulation with the observations of the coherence magnitude and phase shifts of π occurs when $j_* \approx 1$, consistent with the fits to the velocity spectrum (Fig. 9). There is a range of j_* values reported in the literature from different environments; in the deep ocean j_* is typically found to be near 3. This example does not demonstrate the universality of the spectral distribution function E_* or the particular value of j_*, but shows the improvement and advantages of using the modified spectral form.

c. *Comparing observations with the modified and GM79 spectra*

The continental shelf example demonstrates the merits of using the modified spectrum for comparing internal wave fields from different environments. Suppose we tried instead to use GM79 for the comparison, how would the three parameters N_0, b, and E be chosen? First, the buoyancy frequency N_0 must really be set to a constant, as is N_{ref}, if one is to compare energy levels in different environments. This is because the energy is referenced to $N = N_0$; it would be confusing to change this reference at each location depending upon local $N(z)$. As a consequence, the definitions of b and N_0 can no longer be directly associated with the exponential form of the local $N(z)$ in (18).

Then one logical way to proceed to fit the remaining two parameters b and E would be to estimate first the

product $N_0 b$ from the integral of $N(z)$, as this is a fundamental quantity scaling the wavenumber bandwidth (20) in the WKB approximation. For CMO the result is $N_0 b = 1.25$ m s^{-1}. Then using a fixed $N_0 = 3$ cph results in $b = 240$ m. The quantity E can then be estimated from the observed spectral levels at high frequency (Fig. 9). The energy per unit mass $Eb^2N_0^2$ is found to be between 1.6 and 4.7 mJ kg^{-1}. Then the resulting E would be 1–3 $\times$ 10^{-3}. Hence, the scaling of GM79 could be used in this situation by fixing N_0 to be a constant 3 cph, choosing b about 5 times less than the canonical 1300 m, and setting E about 15–45 times larger than canonical. However, the pathway to estimate these parameters is not unique—if a different procedure were used to estimate these scales, then different values would result. Using the modified spectral form with scales E_{ref} and $D(\omega)$ and an unambiguously defined N_{ref} clarifies the physical meaning of the parameters and simplifies comparing internal wave fields from diverse environments.

5. Discussion and summary

A modified version of the GM79 statistical representation of the internal wave field is presented to clarify the normalization of the energy spectrum, modify the frequency dependence below the semidiurnal tidal band, and account explicitly for turning points and boundaries. The motivation for developing this modification is to facilitate comparisons among observed internal wave fields in different water depths, stratifications, and latitudes. There have been many studies comparing internal wave energy based on spectral observations (e.g., Roth et al. 1981; Wunsch 1976; Levine et al. 1985). The modified spectrum provides a consistent framework to interpret these results and future comparisons.

The scaling of the GM79 formulation with the parameters E, b, and N_0, is difficult to apply to diverse environments with different $N(z)$ and water depth. In the original formulation by GM, the scales for time ($1/N_0$) and depth (b) were determined from the buoyancy frequency profile (18). This results in the total energy per unit mass scaling as

$$Eb^2N_0^2\frac{N(z)}{N_0}$$

as these are the only dimensional scales used. The nondimensional E is then the fraction of this scaled total energy per unit mass actually present in the wave field. However, it is not clear if N_0 and b should be determined from the N profile alone or if other data should be used. This leads to ambiguity in interpreting the parameters from observations.

In the modified spectrum (26) no analogous energy scaling is proposed and different oceans are compared based on the dimensional parameter E_{ref} (Table 1). Energy per unit mass was chosen as the reference scale (for $N_{\text{ref}} > \omega > \omega_{S_2}$) as it seems to be the quantity that is nearly constant throughout the ocean, rather than, say, energy per unit area. This is demonstrated in the example from the continental shelf (Fig. 9). It may be that there exists an underlying fundamental scaling that would explain variations in E_{ref}; this issue is left for future study. The modified spectral parameterization with the two independent scales E_{ref} and $D(\omega)$ is easier to apply to observations and provides consistent comparison among wave fields in diverse environments.

The latitudinal dependence is also modified to clarify the frequency bandwidth in the spectral formulation and to improve comparison with observations at low latitude. Rather than force the integral of $B(\omega)$ from f to N to be constant as in (25), a modified $\hat{B}(\omega)$ form is proposed that is normalized by the integral from ω_{S_2} to N_{ref} [(27), (28)], forcing the level of the frequency spectrum above ω_{S_2} to be essentially constant with f. The consequence of using $\hat{B}$ is that the total energy (integrated from f to N) increases as f decreases (Fig. 2). Using $\hat{B}$ also improves the agreement of the spectral shape with observations at frequencies below the semidiurnal tidal band (Fig. 6).

The modified spectrum explicitly includes the effects of the boundaries and vertical turning points by creating WKB modes (Fig. 1). The resulting statistical quantities are based on the assumption that amplitudes of different vertical modes are statistically independent. The effects of the boundaries and turning points appear to be important in observations from the upper ocean and the continental shelf (Figs. 9 and 10). In situations where it is desirable to use exact numerical modal solutions rather than a WKB approximation, the normalization function $Q(\omega)$ [(6)] should be set to the waveguide thickness $D(\omega)$ [(14)] to ensure consistent comparisons with spectra using WKB modes.

The specific choice of E_* presented here may not be the optimal representation of the wave field, other forms could be substituted into this modified spectral framework. For example, it is not necessary to assume that E_* is separable into a product of a function of ω and a function of j—there is evidence that the wavenumber bandwidth is a function of frequency (e.g., Pinkel 1984). Vertically propagating solutions could be included while still retaining most aspects of the E_* parameterization. It is also straightforward to allow for horizontal anisotropy, as is often observed on the continental shelf. The vertical structure function could also be modified to accommodate the effects of mean vertical shear (e.g., Boyd et al. 1993; Peters 1983).

Although the main objective of this paper is to present a framework to improve and clarify the parameterization of the random internal wave field, some preliminary conclusions can be attempted. While the ''universality'' of the internal wave spectral continuum has been known for a long time, it appears that it is the level of energy per unit mass that is nearly invariant. This conclusion is based on analysis of a few observations from wave fields measured in diverse environments, such as the

deep ocean at low latitude and the shallow continental shelf. The modified spectrum should simplify further comparisons and perhaps contribute toward answering the ongoing question of what dynamical processes are most important in maintaining this background level of internal waves. Another use of the modified spectrum is to clarify the continuum portion of the spectrum so that deviations can be more consistently identified. Deviations could be within the continuum band itself, such as horizontally anisotropy, or at energetic narrow bands at tidal, near-inertial, or near-buoyancy frequencies. In fact, the processes responsible for generating these deviations could be the sources of energy for maintaining the continuum itself.

Acknowledgments. Valuable comments provided by Tim Boyd, Mike Gregg, Eric Kunze, and the anonymous reviewers are much appreciated. The support by the Office of Naval Research (N00014-95-1-0534) and the enthusiasm of program manager Lou Goodman are gratefully acknowledged.

APPENDIX

Spectral Quantities

This appendix presents the most useful spectral quantities using $E(\omega, \theta, j)$ for the modified spectrum (23) as well as GM79 [(19)]. Some of the spectral quantities can be simplified by using the following relationship for the sum:

$$J \sum_{j=1} \frac{\cos 2\pi j\chi}{j^2 + j_*^2} = F(\chi) - 1, \tag{A1}$$

where

$$F(\chi) = 2 - \frac{\pi j_* \left\{ \cosh(\pi j_*) - \cosh\left[2\pi j_* \left(\chi - \frac{1}{2} \right) \right] \right\}}{\pi j_* \cosh(\pi j_*) - \sinh(\pi j_*)} \tag{A2}$$

and

$$\frac{1}{J} = \frac{1}{2j_*^2}(\pi j_* \coth \pi j_* - 1). \tag{A3}$$

a. Moored spectrum (MS)

Using (35) the $\mathrm{MS}(\omega)$ can be written as

$$\mathrm{MS}^{11}_{\mathrm{GM79}} = \mathrm{MS}^{22}_{\mathrm{GM79}} = \frac{1}{2} E b^2 N_0^2 \left(\frac{N}{N_0} \right) \left(\frac{\omega^2 + f^2}{\omega^2} \right) B(\omega) \tag{A4}$$

$$\mathrm{MS}^{11}_{*} = \mathrm{MS}^{22}_{*} = \frac{1}{2} E_{\mathrm{ref}} \left(\frac{N}{N_{\mathrm{ref}}} \right) \left(\frac{\omega^2 + f^2}{\omega^2} \right) \hat{B}(\omega) F\left(\frac{\xi}{D} \right) \tag{A5}$$

$$\mathrm{MS}^{33}_{\mathrm{GM79}} = E b^2 N_0^2 \left(\frac{N}{N_0} \right) \left(\frac{\omega^2 - f^2}{\omega^2} \right) B(\omega) \tag{A6}$$

$$\mathrm{MS}^{33}_{*} = E_{\mathrm{ref}} \left(\frac{N}{N_{\mathrm{ref}}} \right) \left(\frac{\omega^2 - f^2}{\omega^2} \right) \hat{B}(\omega) \left[2 - F\left(\frac{\xi}{D} \right) \right]. \tag{A7}$$

b. Dropped spectrum (DS)

Using (36) the $\mathrm{DS}(j)$ can be written as

$$\mathrm{DS}^{11}_{\mathrm{GM79}} = \mathrm{DS}^{22}_{\mathrm{GM79}} = \frac{3}{4} E b^2 N_0^2 H(j) \tag{A8}$$

$$\mathrm{DS}^{11}_{*} = \mathrm{DS}^{22}_{*} = \frac{E_{\mathrm{ref}}}{2} H(j) \left[\int_f^{N_{\max}} \frac{\omega^2 + f^2}{\omega^2} \hat{B}(\omega)\, d\omega \right] \tag{A9}$$

$$\mathrm{DS}^{33}_{\mathrm{GM79}} = \frac{1}{2} E b^2 N_0^2 H(j) \tag{A10}$$

$$\mathrm{DS}^{33}_{*} = E_{\mathrm{ref}} H(j) \left[\int_f^{N_{\max}} \frac{\omega^2 - f^2}{\omega^2} \hat{B}(\omega)\, d\omega \right]. \tag{A11}$$

c. Moored vertical coherence (MVC)

The $\mathrm{MVC}(\omega, z_1, z_2)$ [(37)] between the same components can be written as

$$\mathrm{MVC}^{11}_{\mathrm{GM79}} = \mathrm{MVC}^{22}_{\mathrm{GM79}} = \mathrm{MVC}^{33}_{\mathrm{GM79}} = F(\epsilon) - 1 \tag{A12}$$

where

$$\epsilon = \frac{|\xi_{\mathrm{GM79}}(z_1) - \xi_{\mathrm{GM79}}(z_2)|}{2b} = \frac{|N(z_1) - N(z_2)|}{2N_0}$$

$$\mathrm{MVC}^{11}_{*} = \mathrm{MVC}^{22}_{*} = \frac{F(\lambda) + F(\gamma) - 2}{F\left[\frac{\xi(z_1)}{D(\omega)} \right]^{1/2} F\left[\frac{\xi(z_2)}{D(\omega)} \right]^{1/2}}, \tag{A13}$$

where

$$\lambda = \frac{\xi(z_1) + \xi(z_2)}{2D(\omega)}, \qquad \gamma = \frac{|\xi(z_1) - \xi(z_2)|}{2D(\omega)}$$

$$\mathrm{MVC}^{33}_{*} = \frac{F(\gamma) - F(\lambda)}{\left\{ 2 - F\left[\frac{\xi(z_1)}{D(\omega)} \right] \right\}^{1/2} \left\{ 2 - F\left[\frac{\xi(z_2)}{D(\omega)} \right] \right\}^{1/2}}. \tag{A14}$$

d. Moored horizontal coherence (MHC)

The $\mathrm{MHC}(\omega, \Delta r)$ (38) can be written as

$$\mathrm{MHC}^{11}_{\mathrm{GM79}} = \sum_j H(j)\left[J_0(\alpha_j\Delta r) - \cos(2\phi)J_2(\alpha_j\Delta r)\left(\frac{\omega^2 - f^2}{\omega_2 + f^2}\right)\right] \tag{A15}$$

$$\mathrm{MHC}^{22}_{\mathrm{GM79}} = \sum_j H(j)\left[J_0(\alpha_j\Delta r) + \cos(2\phi)J_2(\alpha_j\Delta r)\left(\frac{\omega^2 - f^2}{\omega_2 + f^2}\right)\right] \tag{A16}$$

$$\mathrm{MHC}^{33}_{\mathrm{GM79}} = \sum_j H(j)J_0(\alpha_j\Delta r) \tag{A17}$$

$$\mathrm{MHC}^{11}_{*} = \frac{\sum_j H(j)\cos^2\left[j\pi\frac{\xi(z)}{D(\omega)}\right]\left[J_0(\alpha_j\Delta r) - \cos(2\phi)J_2(\alpha_j\Delta r)\left(\frac{\omega^2 - f^2}{\omega^2 + f^2}\right)\right]}{\sum_j H(j)\cos^2\left[j\pi\frac{\xi(z)}{D(\omega)}\right]} \tag{A18}$$

$$\mathrm{MHC}^{22}_{*} = \frac{\sum_j H(j)\cos^2\left[j\pi\frac{\xi(z)}{D(\omega)}\right]\left[J_0(\alpha_j\Delta r) + \cos(2\phi)J_2(\alpha_j\Delta r)\left(\frac{\omega^2 - f^2}{\omega^2 + f^2}\right)\right]}{\sum_j H(j)\cos^2\left[j\pi\frac{\xi(z)}{D(\omega)}\right]} \tag{A19}$$

$$\mathrm{MHC}^{33}_{*} = \frac{\sum_j H(j)\sin^2\left[\frac{j\pi}{D(\omega)}\xi(z)\right]J_0(\alpha_j\Delta r)}{\sum_j H(j)\sin^2\left[\frac{j\pi}{D(\omega)}\xi(z)\right]}. \tag{A20}$$

REFERENCES

Blumenthal, M. B., and M. G. Briscoe, 1995: Distinguishing propagating waves and standing modes: An internal wave model. *J. Phys. Oceanogr.*, **25,** 1095–1115.

Boyd, T. J., D. S. Luther, R. A. Knox, and M. C. Hendershott, 1993: High-frequency internal waves in the strongly sheared currents of the upper equatorial Pacific: Observations and a simple spectral model. *J. Geophys. Res.*, **98,** 18 089–18 107.

——, M. D. Levine, and S. R. Gard, 1997: Mooring observations from the Mid-Atlantic Bight, July–September 1996. Data Rep. 164, Ref. 97-2, Oregon State University, 226 pp.

Colosi, J. A., and the ATOC Group, 1999: A review of recent results on ocean acoustic wave propagation in random media: Basin scales. *IEEE J. Oceanic Eng.*, **24,** 138–155.

Desaubies, Y. J. F., 1973: Internal waves near the turning point. *Geophys. Fluid Dyn.*, **5,** 143–154.

——, 1976: Analytical representation of internal wave spectra. *J. Phys. Oceanogr.*, **6,** 976–981.

Eriksen, C. C., 1980: Evidence for a continuous spectrum of equatorial waves in the Indian Ocean. *J. Geophys. Res.*, **85,** 3285–3303.

Flatté, S. M., 1979: *Sound Transmission through a Fluctuating Ocean.* Cambridge University Press, 299 pp.

Fu, L.-L., 1981: Observations and models of inertial waves in the deep ocean. *Rev. Geophys. Space Phys.*, **19,** 141–170.

Garrett, C. J., and W. Munk, 1972: Space–time scales of internal waves. *Geophys. Fluid Dyn.*, **2,** 255–264.

——, and ——, 1975: Space–time scales of internal waves: A progress report. *J. Geophys. Res.*, **80,** 291–297.

Henyey, F. S., J. Wright, and S. M. Flatté, 1986: Energy and action flow through the internal wave field: An eikonal approach. *J. Geophys. Res.*, **91,** 8487–8495.

Hibiya, T., Y. Niwa, and K. Fujiwara, 1998: Numerical experiments of nonlinear energy transfer within the oceanic internal wave spectrum. *J. Geophys. Res.*, **103,** 18 715–18 722.

Käse, R. H., and G. Siedler, 1979: Internal wave kinematics in the upper tropical Atlantic. *Deep-Sea Res.*, **26** (GATE Suppl. I), 161–189.

Levine, M. D., 1991: Observing oceanic internal waves: What have we learned? What can we learn? *The Dynamics of Oceanic Internal Waves: Proc. 'Aha Huliko'a Hawaiian Winter Workshop*, Honolulu, HI, University of Hawaii at Manoa, 467–480.

——, 1999: Internal waves on the continental shelf. *Internal Wave Modelling: Proc. 'Aha Huliko' a Hawaiian Winter Workshop*, Honolulu, HI, University of Hawaii at Manoa, 1–8.

——, C. A. Paulson, M. G. Briscoe, R. A. Weller, and H. Peters, 1983: Internal waves in JASIN. *Philos. Trans. Roy. Soc. London*, **A308,** 389–405.

——, ——, and J. H. Morison, 1985: Internal waves in the Arctic Ocean: Comparison with lower-latitude observations. *J. Phys. Oceanogr.*, **15,** 800–809.

McPhaden, M. J., and Coauthors, 1998: The Tropical Ocean-Global Atmosphere observing system: A decade of progress. *J. Geophys. Res.*, **103,** 14 169–14 240.

Müller, P., and G. Siedler, 1976: Consistency relations for internal waves. *Deep-Sea Res.*, **23,** 613–628.

——, and M. Briscoe, 1999: Diapycnal mixing and internal waves. *Dynamics of Oceanic Internal Gravity Waves: Proc. 'Aha Huliko' a Hawaiian Winter Workshop*, Honolulu, HI, University of Hawaii at Manoa, 289–294.

——, D. J. Olbers, and J. Willebrand, 1978: The IWEX spectrum. *J. Geophys. Res.*, **83,** 479–500.

——, G. Holloway, F. Henyey, and N. Pomphrey, 1986: Nonlinear interactions among internal gravity waves. *Rev. Geophys.*, **24,** 493–536.

Munk, W., 1980: Internal wave spectra at the buoyant and inertial frequencies. *J. Phys. Oceanogr.*, **10,** 1718–1728.

——, 1981: Internal waves and small-scale processes. *Evolution of Physical Oceanography,* B. A. Warren and C. Wunsch, Eds., The MIT Press, 264–290.

——, and C. Wunsch, 1998: Abyssal recipies II: Energetics of tidal and wind mixing. *Deep-Sea Res.*, **45,** 1977–2010.

Neyfeh, A. H., 1973: *Perturbation Methods.* John Wiley and Sons, 425 pp.

Peters, H., 1983: The kinematics of a stochastic field of internal waves modified by a mean shear current. *Deep-Sea Res.*, **30,** 119–148.

Pinkel, R., 1984: Doppler sonar observations of internal waves: The wavenumber-frequency spectrum. *J. Phys. Oceanogr.*, **14,** 1249–1270.

——, A. Plueddemann, and R. Williams, 1987: Internal wave observations from FLIP in MILDEX. *J. Phys. Oceanogr.*, **17,** 1737–1757.

Polzin, K. L., J. M. Toole, and R. W. Schmitt, 1995: Finescale parameterizations of turbulent dissipation. *J. Phys. Oceanogr.*, **25,** 306–328.

Roth, M. W., M. G. Briscoe, and C. H. McComas III, 1981: Internal waves in the upper ocean. *J. Phys. Oceanogr.*, **11,** 1234–1247.

Schott, F., and J. Willebrand, 1973: On the determination of internal-wave directional spectra from moored instruments. *J. Mar. Res.*, **31,** 116–134.

Willebrand, J., P. Müller, and D. J. Olbers, 1977: Inverse analysis of the Trimoored Internal Wave Experiment (IWEX). *Ber. Inst. Meeereskde.*, **20a,** 117 pp.

Wunsch, C., 1975: Deep ocean internal waves: What do we really know? *J. Geophys. Res.*, **80,** 339–343.

——, 1976: Geographical variability of the internal wave field: A search for sources and sinks. *J. Phys. Oceanogr.*, **6,** 471–485.